J. Electroanal. Chem., 94 (1978) 123—145

ELECTROCHEMICAL REDUCTION OF URACIL IN DIMETHYL SULFOXIDE

AUTOPROTONATION OF THE ANION RADICAL

TIMOTHY E. CUMMINGS * and PHILIP J. ELVING

The University of Michigan, Ann Arbor, Mich., 48109 (U.S.A.)

(Received 8th March 1978; in revised form 2nd May 1978)

ABSTRACT

The electrochemical reduction of uracil in dimethyl sulfoxide was investigated, using d.c. and a.c. polarography, cyclic voltammetry, and controlled potential electrolysis. Uracil is reduced in a one-electron step ($E_{1/2}$ = —2.3 V); the apparent number of electrons transferred (n) decreases from one at infinite dilution to one-half at concentrations above 1 mM. The concentration dependent n-value is due to proton transfer by the parent compound to the radical anion formed on reduction. Such a proton transfer, which has been observed for 2-hydroxypyrimidine, deactivates part of the uracil, which would otherwise be available for reduction, by formation of the more difficultly reducible conjugate base. The uracil anion forms insoluble mercury salts, producing two oxidation waves ($E_{1/2}$ of —0.1 and —0.3 V); the latter wave is due to formation of a passivating film on the electrode. Digital simulations indicate that the protonation rate exceeds $10^5\ M^{-1}s^{-1}$ and that, at low uracil concentration, some of the free radical formed on protonation is further reduced. At concentrations exceeding 1 mM, all of the free radical dimerizes. The effect of added acids and base on the electrochemical behavior is described.

INTRODUCTION

Although considerable progress has been made in understanding the electrochemical behavior of biologically important pyrimidines and purines, and their nucleosides and nucleotides [1—3], several pyrimidines and purines have eluded mechanistic study due to the absence of faradaic response in aqueous media. The reducibility of uracil (2,4-dihydroxypyrimidine) and thymine (2,4-dihydroxy-5-methylpyrimidine) in anhydrous dimethylformamide has been reported [4]; however, no published results are available. Uracil and thymine are important because their nucleotides occur in RNA and DNA, respectively. Uracil nucleotides also serve a minor role in energy transfer reactions; uridine-5′-diphosphate (UDP) is the main carrier of sugar residues, particularly as UDP-D-glucose, in the biosynthesis of polysaccharides or energy storage polymers, e.g., glycogen, in higher animals [5].

The electrochemical reduction mechanisms of uracil and thymine are of particular interest because their catabolism proceeds via an initial two-electron (2e) reduction by NAD(P)H. Additionally, the biological degradation of cytosine,

* Present address: Department of Chemistry, University of Miami, Coral Gables, Fla., 33124, U.S.A.

after hydrolysis and deamination to form uracil, proceeds via the uracil catabolic pathway.

Wasa and Elving [6] investigated the reduction mechanism of 2-hydroxypyrimidine (2-HP) in dimethyl sulfoxide (DMSO); the radical anion, formed on reduction of 2-HP, chemically reacts with unreduced 2-HP to produce the neutral free radical which rapidly dimerizes and the conjugate base of 2-HP. Dimerization of the radical anion, which competes with the proton transfer reaction, appears to occur more slowly than the latter. The information regarding 2-HP reduction should aid in elucidating the uracil reduction mechanism, due to the similarity of the two compounds. The primary distinction between 2-HP and uracil is the absence of an available nitrogen site for intermolecular protonation in uracil, since the keto-enol equilibrium of uracil lies very far to the right in aqueous media (cf. ref. 7 and references cited therein):

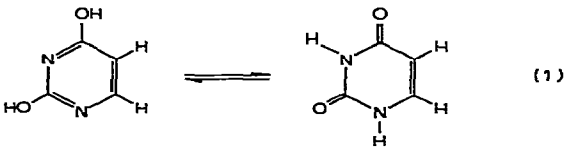

(1)

Proton n.m.r. studies indicate that the lactam form predominates in DMSO as well [8].

EXPERIMENTAL

Chemicals

Uracil was obtained from Calbiochem. Reagent grade tetra-n-butylammonium perchlorate (TBAP) (G. Frederick Smith) was vacuum dried at 60°C for 48 h. An aqueous 20% solution of tetraethylammonium hydroxide (TEAH) (Aldrich) served as a source of hydroxide. Reagent grade acetic acid (Dupont), phenol (Mallinckrodt), perchloric acid (G. Frederick Smith), phosphoric acid (Baker & Adamson), chloroacetic acid (Dow "Specially Purified"), benzoic acid (Baker), and hydroquinone (Baker) served as proton donors. DMSO (Fisher Scientific (certified ACS), Mallinckrodt (analytical reagent) and Baker ("Baker Analyzed" reagent)) was purified by fractional freezing similarly to a technique used to purify pyridine [9]; the cooling bath was H_2O maintained at 12°—14°C. Mercury for electrodes was distilled.

Apparatus

The potentiostat, built in-house, was used with a three-compartment, jacketed electrochemical cell thermostatted at 25°C, except as noted. The hanging mercury drop electrode was a Metrohm E 410 micro feeder (Brinkmann Instruments). A PAR 122 lock-in amplifier (Princeton Applied Research) served as an a.c. modulation voltage source and phase-selective detector for a.c. polarography. Cyclic voltammetric triangular wave forms were obtained from a Wavetek Model 112 function generator. Data were acquired on a Moseley Model 7001A(S) XY recorder or a Tektronix Type 502A oscilloscope. Potentials were

monitored by a Hewlett-Packard Model 3440A digital voltmeter with a Model 3443A auto-range unit. A Unitmetrics Model 1010 10-μl syringe was used for addition of acid and base solutions. Ultraviolet spectra were run on a Beckman Model 25 spectrophotometer using Fisher 1.00-cm silica cells with Teflon caps.

Procedures

Solutions, in which the background electrolyte was 0.1 *M* TBAP, were deoxygenated by purging with purified N_2 for ca. 30 min; an N_2 atmosphere was maintained in the cell throughout data acquisition. Where required, solutions of acids, prepared by dilution of concentrated acids to 3 to 6 *M* in DMSO, or the aqueous TEAH solution were added to the cell; preliminary experiments showed that the amounts of water involved had no effect on the voltammetric behavior. D.c. polarographic data were obtained at a controlled drop-time of 2.07 s, using capillaries with a mercury flow rate (m) at open circuit of 0.80 or 0.48 mg s^{-1} (data obtained with the latter capillary were mathematically adjusted to correlate with conditions at the former capillary, based on the results for 1 m*M* uracil obtained at both capillaries). A new Hg drop was used for each cyclic voltammogram. Because of indications that electrochemical products tenaciously adhered to the electrode, N_2 was used to stir the solution between voltammograms so as to remove the reaction products.

For controlled potential electrolysis, a mercury pool, ca. 0.5 cm deep and 1 cm diameter, was placed in the cell. Separate electrolyses were performed on 10.0 ml of background and uracil solutions. The current-time profile was recorded on an XY recorder, using the x-axis in a time base mode. During electrolysis, N_2 was used to continously stir the solution.

Potentials were measured against a modified aqueous saturated calomel electrode (SCE) by the following system: SCE|saturated KCl in water-methylcellulose bridge with asbestos fiber.

Cyclic voltammetric peak charge calculation

Because of the apparent filming nature of some faradaic peaks, the charge, Q, passed in faradaic cyclic voltammetric peaks was determined as follows. The peak area on the read-out record was defined by extrapolation of the charging current to form a baseline beneath the peak; integration was performed over the potential span from the foot of the peak to the peak potential for peaks Ic and IIa (see Fig. 3 for peak designations) and from the foot of the peak to the potential at which the current returned to the baseline for peaks Ia and IIc; the integrated area in square inches (measured by a Gelman Model 39231 planimeter) was multiplied by the read-out device x- and y-axis sensitivities in V in^{-1} and μA in^{-1} to convert the area units to μA—V; the area in μA—V was divided by the potential scan rate in V s^{-1} to yield the charge passed in μC. In the case of data presented in Fig. 7 and Table 3, integration of the peak IIa area was performed from the foot of the peak to the switching potential for the positive scan and from the switching potential to the point at which the current crossed the baseline for the negative scan.

RESULTS AND DISCUSSION

In the following discussion, Figures and Tables, Roman numbers are used to designate waves and peaks with appended a or c referring to anodic or cathodic processes, respectively.

D.c. polarography

The concentration-dependence of the diffusion current constant ($I_d = \bar{i}_l/cm^{2/3}t^{1/6}$) for uracil is shown in Fig. 1; extrapolation of the results at low concentration to infinite dilution yields an I_d of 1.29 ± 0.04 $\mu A\ s^{1/2}\ mM^{-1}\ mg^{-2/3}$, which corresponds to a diffusion coefficient, D, of $4.5 \times 10^{-6}\ cm^2\ s^{-1}$. Use of the Matsuda equation [10], in which shielding effects are considered and which best describes the i_d—t behavior at controlled drop-times [11], gives a D of 4.0×10^{-6}. The results at c exceeding 1 mM yield an I_d of 0.67.

$E_{1/2}$ shifts from −2.34 V at c below 0.2 mM to −2.32 V at 0.2 to 1 mM, and −2.31 V above 1 mM. Since the uncertainty in $E_{1/2}$ is 0.01 V, this shift is within experimental error; however, the shift parallels the concentration-dependence of I_d and may, therefore, be real.

Between 25° and 50°C, i_l for 1 mM uracil linearly increases with temperature (1.44% $°C^{-1}$) and $E_{1/2}$ becomes more positive (1.2 mV $°C^{-1}$). Because of the very low interfacial surface tension at potentials on the uracil limiting current plateau, the relation of i_l and mercury column-height (h) could not be investigated over a useful range of h.

The concentration-dependence of I_d indicates that the uracil reduction is not a simple electron-transfer but must involve coupled second-order or greater chemical reactions. Based on the viscosities of DMSO, η [12], the product $i_l\eta^{1/2}$ varies

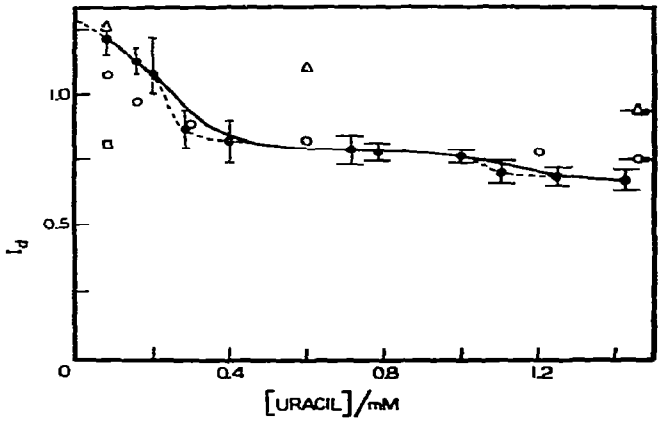

Fig. 1. Concentration-dependence of the d.c. polarographic diffusion current constant (I_d) for uracil, based on mean polarographic currents. Solid circles are experimental results; uncertainties are one standard deviation based on maximum uncertainties (assumed equal to three standard deviations) of all parameters. Triangles are results of digital simulations for reaction of eqn. (2), using $k_1 = 10^3\ M^{-1}\ s^{-1}$; open circles are those using $k_1 = 10^4\ M^{-1}\ s^{-1}$; the square is for $k_1 = 10^5\ M^{-1}\ s^{-1}$; the points with horizontal arrows are for 2.0 mM.

from 1.20 at 25°C to 1.32 at 45°C; this slight temperature dependence suggests that i_l is nearly diffusion controlled; however, Fig. 1 clearly indicates that i_l is not solely diffusion controlled.

The I_d—c behavior indicates that uracil may be reduced via a mechanism similar to that of 2-HP, whereby the reduced species, a radical anion, abstracts a proton from uracil to form the neutral free radical, which rapidly dimerizes, and the conjugate base of uracil. The protonation reaction, which, based on the experimental results (e.g., Fig. 1), must be more rapid than the radical anion dimerization, necessarily reduces the amount of uracil available at the electrode surface for reduction, resulting in an observed I_d smaller than the 1.3 expected for a 1e transfer [6]. Based on results to be presented, the uracil conjugate base reacts with mercury to yield an anodic wave due to formation of a mercury uracil salt.

The slight deviation of the temperature dependence of $i_l\eta^{1/2}$ from that expected for diffusion control is probably due to one or both of the following: (a) on the limiting current plateau, the supply of protonating agent, uracil, is limited by diffusion; (b) the rates of diffusion of uracil and of formation of proton acceptor, (i.e., radical anion) both increase with temperature, resulting in countering forces of reducible species supply and non-faradaic proton transfer consumption of that species.

Controlled potential electrolysis

Controlled potential electrolysis (c.p.e.) at −2.350 V was conducted on 10.0 ml of 2.462 ± 0.035 mM uracil. Similar electrolysis of the background solution gave a linear ln i vs. t plot. The reduction current for uracil, i_u, at any time, t_i, was assumed to be the difference between the total current and that at time t_i for the background. The ln i_u vs. t relation was linear over a period of 7000 s; $i_u/(i_u)_o = 0.06$ at $t = 7000$ s. (A large initial current, which decayed during the first 60 s of both background and uracil electrolyses, is attributed to HgO reduction.) Integration of the ln i_u vs. t plot yielded a faradaic n of 0.503 ± 0.015; the uncertainty is one standard deviation based on standard deviations of the slopes and intercepts for the uracil and background electrolyses. The I_d of 0.67 for a 2.46 mM uracil solution is 52% of the extrapolated low concentration limit of 1.29; thus, an I_d of 1.29 for uracil corresponds to a 1e transfer in agreement with previous reports for DMSO [6]. Because n is concentration-dependent and does not exceed unity, some of the uracil must be rendered electroinactive via a concentration-dependent chemical reaction.

The d.c. polarographic and cyclic voltammetric patterns for the uracil solution before and after electrolysis are shown in Fig. 2. Addition of TEAH in a 1 : 1 ratio with uracil for a 1.25 mM uracil solution produced d.c. polarographic and cyclic voltammetric results identical with those obtained after electrolysis of 2.46 mM uracil.

Cyclic voltammetry

Typical cyclic voltammograms for uracil are shown in Figs. 2B and 3. The absence of an anodic peak at potentials negative of −2 V indicates that either the uracil electron-transfer process is not reversible or a chemical reaction is

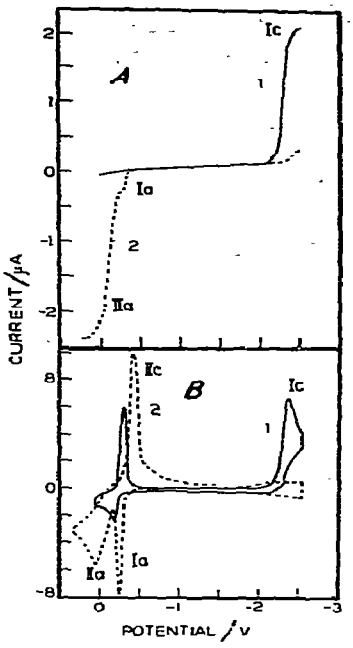

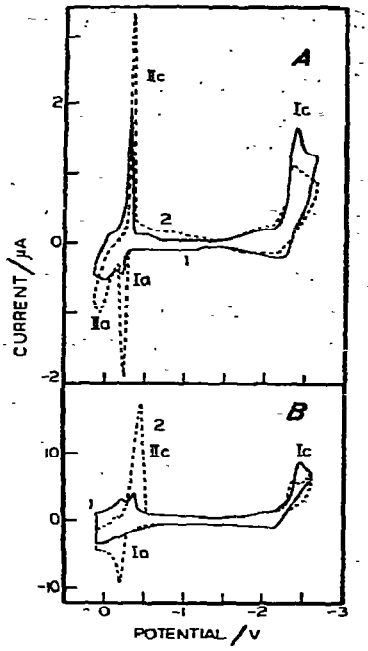

Fig. 2. D.c. polarographic and cyclic voltammetric behavior of a 2.462 m*M* uracil solution. Curves 1 (solid lines) are before controlled potential electrolysis; curves 2 (dashed lines) are after electrolysis. (A) D.c. polarograms with 2.07 s drop-time and 0.80 mg s^{-1} mercury flow rate. (B) Cyclic voltammograms with 0.48 V s^{-1} scan rate and 0.0153 cm^2 electrode area.

Fig. 3. Effect of added base on the cyclic voltammetric behavior of 1.00 m*M* uracil solution. Curves 1 (solid lines) are without added base; curves 2 (dashed lines) are with 0.4 m*M* tetraethylammonium hydroxide present. Electrode area is 0.0153 cm^2; scan rate is (A) 0.106 V s^{-1} and (B) 3.66 V s^{-1}.

consuming the reduction product. Peaks Ia, IIa and IIc, which do not appear if the negative potential limit of the cyclic scan (E_λ) is positive of the uracil reduction potential region, are, therefore, associated with a uracil species and substantiate the involvement of coupled chemical reactions, as suggested by the I_d concentration-dependence and n of 0.5 at high concentrations.

As the positive E_λ is shifted to more negative potential but remains positive of the potential at which Ia occurs, peak IIc decreases; hence, species formed in the IIa process must be involved in the IIc process. Further, since IIc does not disappear unless E_λ is at a potential negative of Ia, species formed in Ia must also be involved in the IIc process. The shape of IIc is indicative of film stripping from the electrode surface; hence, Ia and IIa are due to film deposition.

The dependency of $i_p/Acv^{1/2}$ for peak Ic on concentration (Fig. 4) shows a trend similar to the I_d—c relation. At a given scan rate (v), the ratio of $i_p/Acv^{1/2}$ for any two concentrations is within 5 to 15% of the corresponding I_d ratio; hence, phenomena responsible for the concentration-dependence of I_d similarly affect the cyclic voltammetric response. The dependence of $i_p/Acv^{1/2}$ on v will be discussed.

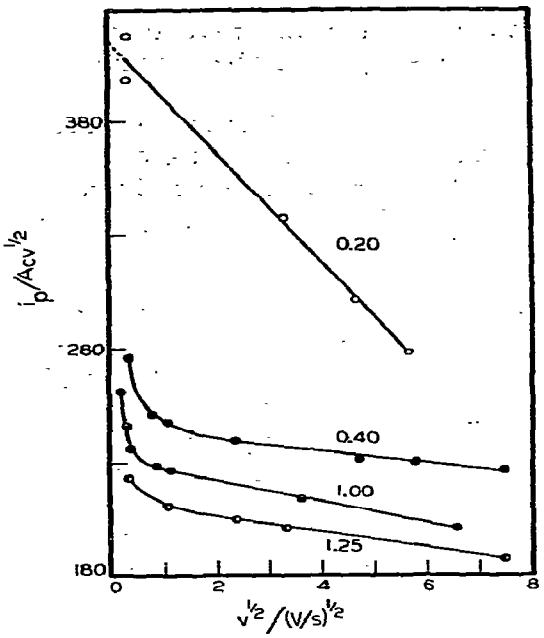

Fig. 4. Cyclic voltammetric reduction peak Ic current function, $i_p/Acv^{1/2}$, dependence on concentration and scan rate (v). Uracil concentrations are shown in millimolar units on the curves.

The Ic peak potential, E_p, varies linearly with log v over the scan rate range of 0.1 to 25 V s^{-1}; however, the slope of the linear relationship is concentration-dependent, ranging from −0.039 V $decade^{-1}$ for 0.4 m*M* to 0.058 V $decade^{-1}$ at 1.25 m*M*. At v = 0.1 V s^{-1}, E_p is −2.39 ± 0.01 V, independent of concentration.

Effect of acid addition

Most common acids, e.g., $HClO_4$, H_3PO_4, $ClCH_2COOH$ and C_6H_5COOH, are reduced (hydrogen ion reduction) more easily than uracil, and, therefore, have no apparent effect on the uracil polarographic wave. Acetic acid, which is reduced at $E_{1/2}$ = −2.5 V, profoundly affects the wave, e.g., at an acetic acid-uracil molar ratio of 7, the apparent uracil polarographic n is 15. Phenol, which is not reduced at potentials positive of background discharge, has an effect similar to, but weaker than, that of acetic acid. Added acid had no significant effect on the uracil $E_{1/2}$.

$E_{1/2}$ for previously studied pyrimidines [2,3,13—17] is dependent on pH in aqueous media and on added proton donor in non-aqueous media; however, the uracil $E_{1/2}$ independence from proton availability is not completely unexpected. In the cases of pyrimidine, cytosine and 2-hydroxypyrimidine, a ring nitrogen is available for protonation or hydrogen bonding interaction; since such bonding facilitates reduction, $E_{1/2}$ is expected to shift positively with increasing proton availability. Since uracil is predominantly in the lactam form, the only sites available for protonation are the exocyclic oxygens, for which an aqueous $pK_a \leqslant 0.5$

has been suggested [18]; consequently, protonation preceding reduction is not expected and the only source for a proton dependency would be a reaction following electron-transfer.

Since the ability of nitrogen heterocycles to lower the hydrogen overpotential is well established [19], the results for uracil reduction with added acetic acid or phenol probably reflect catalytic hydrogen discharge involving a uracil reduction product. The positive shift of $E_{1/2}$ with decreasing pH for pyrimidine, cytosine and 2-hydroxypyrimidine avoids interference of the catalytic process in these reductions.

It is unlikely that protonation by residual water in the solvent plays an appreciable role in the observed behavior of uracil. This statement is supported by a variety of considerations, e.g., the relatively minor effect seen on addition of phenol which is a very much stronger acid than water (at 1 : 1 phenol : uracil ratio, the apparent n is 0.7 compared to 0.6 in the absence of phenol), the lack of any appreciable effect of added water on the reduction of 2-hydroxypyrimidine in DMSO until the water exceeded 1% by volume [6], and the major difference in the competitive rates of reaction of the pyrimidine radical anion in non-aqueous medium for dimerization ($8 \times 10^5\ M^{-1}\ s^{-1}$) and for proton abstraction from water ($7\ M^{-1}\ s^{-1}$) [14].

Effects of base addition

Addition of base (TEAH) decreased wave Ic and produced waves Ia and IIa with $E_{1/2}$ of —0.3 and —0.1 V, respectively (Fig. 5; Table 1); corresponding cyclic voltammetric results are given in Fig. 3 and Table 2.

Manousek and Zuman [20] observed two anodic waves due to uracil in aqueous Britton-Robinson buffers for pH above 7. The more negative wave's $E_{1/2}$ was slightly dependent on uracil concentration and varied as —0.066 pH from pH 7 to pH 9.5 (it was ca. 0.2 V at pH 7); above pH 9.5, $E_{1/2}$ varied as —0.033

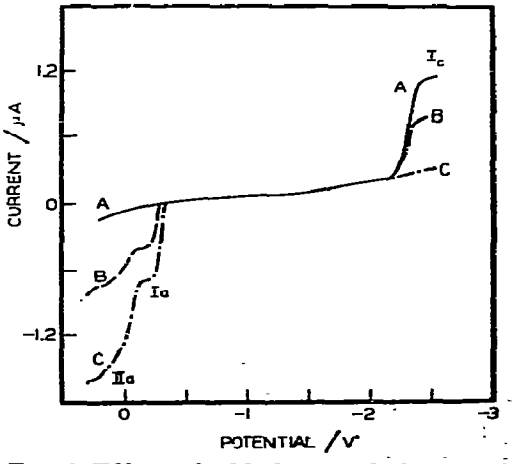

Fig. 5. Effect of added tetraethylammonium hydroxide (TEAH) on the d.c. polarographic behavior of 1.25 m*M* uracil. Conditions: 2.07 s drop-time and 0.80 mg s^{-1} mercury flow rate. (A) 0.0 m*M* TEAH, (B) 0.51 m*M* TEAH, (C) 1.06 m*M* TEAH.

TABLE 1

Variation of the DME waveheights for uracil on addition of TEAH

[Uracil]/m*M*	[TEAH]/m*M*	i_l for wave			
		Ic/μA	Ia/μA	IIa/μA	I_d [a]
0.30	0	0.30	0	0	0.89
0.30	0.13	0.25	0.12	0.07	1.29
0.30	0.30	0.15	0.23	0.10	1.41
1.00	0	0.86	0	0	0.76
1.00	0.40	0.52	0.41	0.16	0.97
1.00	0.94	≤0.12	0.34	1.06	1.34
1.25	0	1.03	0	0	0.73
1.25	0.51	0.75	0.48	0.27	1.06
1.25	1.01	0.35	0.33	1.16	1.30
1.25	1.06	0.28	0.33	1.24	1.31

[a] Summation diffusion current constant for waves Ic, Ia and IIa.

pH; the limiting current increased linearly with concentration and levelled off at 0.12 mM uracil. The more positive wave did not plateau by the positive potential background discharge. The waves, attributed to formation of a mercury salt [20], presumably involve salt formation with a uracil anion.

Ultraviolet absorption spectra of uracil show that deprotonation occurs in water at N(1) and N(3) to about the same extent [21,22]; however, the relative proportions appear to be dependent on buffer nature and dielectric constant of the medium [22]. Addition of TEAH would be expected to generate R^- from uracil, RH. The appearance of waves Ia and IIa, with a concomitant decrease in Ic, upon base addition indicates that uracil is being chemically converted to a

TABLE 2

Variation of the cyclic voltammetric peak areas (charge passed) for uracil on addition of TEAH [a]

[Uracil]/m*M*	[TEAH]/m*M*	(Q/A [b])/μC cm^{-2}, for peak		
		Ic	Ia	IIa
0.30	0	23	0	9
0.30	0.15	21	21	36
0.30	0.30	11	41	31
1.00	0	84	13	38
1.00	0.40	36	71	58
1.00	0.94	0	75	121
1.25	0	94	9	26
1.25	0.51	46	69	72
1.25	1.06	23	73	171

[a] Scan rate (v) = 0.102 V s^{-1} for 0.3 and 1.25 m*M*, and 0.106 V s^{-1} for 1.0 m*M*.
[b] See Experimental section for procedure used to convert peak area to charge, Q; A refers to the electrode area (0.0153 cm^2).

non-reducible species, R^-, and that waves Ia and IIa are related to R^-, probably through mercury salt formation.

Tables 1 and 2 indicate that wave Ia and peak Ia reach limiting values of about $i_l = 0.4\ \mu A$ and Q/A of 70 to 80 $\mu C\ cm^{-2}$, respectively. Wave Ia appears to be associated with filming, as the current profile during the drop-life shows a t^M relation with $M < 0$. The fact that peak Ia reaches a limiting value with increasing R^- concentration indicates surface saturation coverage by the film.

Product characterization

Characterization of the products is largely based on deductions from the faradaic patterns seen on reduction, the behavior of solutions resulting from preparative electrolysis, the well-characterized products obtained from related pyrimidines, the reported products obtained on radiolysis, and theoretical deductions based on electronic structure. Although it would have been informative to have isolated individual dimeric and dihydrouracil products and to have determined their structure, it was not feasible to do so, e.g., chromatography of exhaustively electrolyzed solutions could not be depended upon to yield definitive results due to product instability; even if such attempts were successful, it would still not be possible to differentiate between anionic products and their protonated forms. Other problems involved include the difficulty of selecting a solvent immiscible with DMSO, which would completely extract the reduction and other reaction products unchanged without removing the background electrolyte, and from which the products could be recovered with their identity unaltered. Product recovery by freeze-drying was impractical due to the relatively large amount of background electrolyte present and to the likelihood of product alteration during evaporation.

Spectral identification of the reduction products would be impractical due to the absence of reference spectra and the instability of the likely reduction products [34]. Spectral data on the uracil anion are subsequently discussed.

Proton n.m.r. examination of DMSO solutions of uracil at the concentrations involved, before or after treatment and reaction, did not yield interpretable results even on attempted decoupling of the DMSO and tetrabutylammonium ion hydrogens.

MECHANISM

The mechanism, which seems best to fit the information available, is shown in Fig. 6. Several aspects of the behavior expected for such a mechanism can be specified. Based on studies of similar compounds [3], k_3 for dimerization of $\dot{R}H_2$ may be of the order of 10^6 to $10^8\ M^{-1}\ s^{-1}$; because of electrostatic repulsion, dimerization of $\dot{R}H^-$ should be slower, e.g., k_2 may be 10^4 to $10^6\ M^{-1}\ s^{-1}$. Because the protonation does not involve reaction between molecules of similar charge with concomitant charge repulsion, and because of the very basic nature of radical anions, protonation of $\dot{R}H^-$ is expected to be more rapid than its dimerization, i.e., k_1 greater than k_2; however, since the protonation does not involve two molecules with the strong reaction tendency of free radicals, e.g., dimerization of $\dot{R}H_2$ where charge repulsion is not involved, the protonation is expected

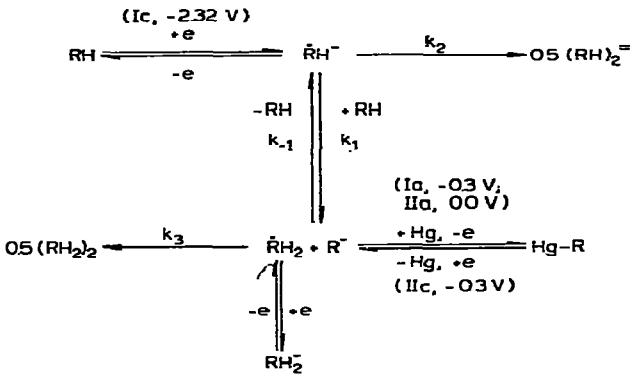

Fig. 6. Reduction mechanism for uracil in DMSO. Symbols: RH, uracil; $\dot{R}H^-$, radical anion; $\dot{R}H_2$, free radical; RH_2^-, reduced free radical; R^-, uracil anion. The k represent rate constants; the Roman numbers are wave and peak designations (cf. Fig. 2). Potentials are for 1.25 mM uracil and are $E_{1/2}$ for Ic, Ia and IIa, and E_{pc} for IIc. For Ia, IIa and IIc, solution is also 1.06 mM in TEAH.

to be slower than dimerization of $\dot{R}H_2$, i.e., k_1 less than k_3. Thus, k_1 may be ca. 10^5 to 10^7 M^{-1} s^{-1}. Because dimerization of $\dot{R}H_2$ is rapid and irreversible, protonation following the initial electron-transfer will be effectively irreversible; hence, the magnitude of k_1 will not affect the mechanistic behavior provided k_{-1} is not comparable in magnitude to k_3.

The mechanism proposed (Fig. 6) is generally similar to that proposed for 2-hydroxypyrimidine (2-HP) [6]; the major difference is the absence of an experimentally observable proton donor effect in the former. As previously discussed, prior protonation of uracil, unlike 2-HP, is not expected because of the predominant lactam tautomer's nature; however, proton donor addition could influence the electrochemical behavior, since the added acid can replace uracil in the protonation of $\dot{R}H^-$, thereby making more uracil available for reduction. Catalytic hydrogen discharge at the uracil reduction potential precludes experimental confirmation of added proton donor involvement in the following protonation step.

Proportions of the uracil anionic tautomers

Nakanishi et al. [21], who used ultraviolet absorption spectrophotometry to investigate the ratio of uracil anionic tautomers present in aqueous solution as a function of pH, report that, at pH 12, 49% of the anion exists as tautomer I which has an absorption maximum at 286 nm; the reported molar absorptivity (ϵ) of 1.22×10^4 M^{-1} cm^{-1}, which is based on that for the neutral species and the ratio of molar absorptivities and ionic forms of 3-methyluracil, was used to compute the fraction of I. A molar absorptivity of 5.82×10^3 M^{-1} cm^{-1} at 258 nm for II was determined by comparison of the uracil anion spectrum with those of 1- and 3-methyluracil anions.

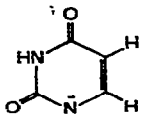

(I)

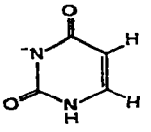

(II)

A 0.043 m*M* uracil in DMSO solution (0.1 *M* TBAP) gives an absorption maximum at 262 nm ($\epsilon = 8.9 \times 10^3\ M^{-1}\ cm^{-1}$); the solvent cut-off begins at 259 nm. The λ_{max} for uracil in DMSO is only 2 nm longer than that in pH 6.7 aqueous solution [21]. Addition of 0.14 m*M* TEAH causes disappearance of the 262-nm peak and appearance of an asymmetric peak with $A = 0.478$ at 296 nm (1.00-cm cell), which, by comparison with the aqueous spectra [21], is due to I; the peak asymmetry is considerably less than that in aqueous solution, which suggests that proton loss occurs principally at N(1).

Since ϵ is unknown for the uracil anions in DMSO, concentrations can be estimated only by analogy to aqueous solution data. On assuming similar peak shapes in DMSO and water for I, the absorbance of this species at various ϵ was calculated from A at 296 nm and the predicted aqueous absorption curve of this tautomer in Fig. 4 of ref. 21; subtraction of this calculated absorbance from the observed absorbance revealed a peak at 265 nm with $A = 0.046$. Use of the aqueous ϵ for the two anion tautomers indicates concentrations of 0.039 and 0.008 m*M* for I and II, respectively; use of the neutral species aqueous ϵ indicates a neutral species concentration of 0.047 m*M* in the solution without TEAH; hence, the sum of the two anionic species concentrations equals that of the original neutral species and 83% of the anion exists as tautomer I. Since the standard deviations for the concentration and cell path-length are far below the 10% required for an apparent 0.004 m*M* error in total uracil concentration, the change from aqueous to DMSO solvent affects the ϵ of all species similarly, i.e., all ϵ are a factor of 8.9/8.1 larger in DMSO than in water; hence, ϵ are $1.34 \times 10^4\ M^{-1}\ cm^{-1}$ and $6.39 \times 10^3\ M^{-1}\ cm^{-1}$ for tautomers I and II, respectively, in DMSO containing 0.1 *M* TBAP.

Because the uracil anions are probably not involved in any equilibria of order higher than one, it is reasonable to assume that the relative proportions of the two anionic tautomers is independent of total uracil concentration, although the ratio may depend on the nature and concentration of supporting electrolyte [22].

Nature of the uracil-mercury film

The precise nature of the mercury-uracil film is unclear. Although a mercury-(I)-uracil salt might be logically expected, formation of Hg(II)-uracil salt may be possible, e.g., binding of Hg(II) to AT-rich DNA has been suggested to occur at N(3) of thymidine [23], and crystal structures of uracil-Hg(II) chloride complexes have been elucidated [24]. The latter complex involves both lateral hydrogen-bonding between uracils in the same plane and hydrogen-bonded base stacking, with a 2 : 1 ratio of uracil : Hg(II). Addition of 0.046 m*M* uracil anion in DMSO to $HgCl_2$ in DMSO (both solutions 0.1 *M* in TBAP) produced no precipitate; hence, the mercury-uracil salt probably involves Hg(I), a fact which could not be confirmed because of the unavailability of a soluble Hg(I) salt (addition of $Hg_2(NO_3)_2$ alone to 0.1 *M* TBAP in DMSO produced a grey precipitate, presumably due to formation of metallic mercury).

Phase-selective a.c. polarography of an electrolyzed uracil solution showed an a.c. peak corresponding to Ia, whose phase angle was considerably less than 45°. Additionally, the capacitive current at potentials positive of Ia was con-

siderably smaller than the coincident a.c. responses for background or unelectrolyzed uracil solutions. The small a.c. phase angle for Ia indicates that Ia is faradaic in nature and, based on the depressed capacitive current, most likely involves film formation.

The shape of cyclic voltammetric peaks involving deposition of an insoluble substance, i.e., film formation, is characteristic [26]; the leading edge of the peak is very steep; the trailing edge decays more slowly with its current-potential relation being described by the error function. This predicted shape is observed for Ia at fast scan rate but not at slow scan rate (Fig. 3); additionally, IIa disappears at fast scan rate.

Because the film generated by Ia reaches a limiting value of ca. 75 μC cm^{-2} and because the trailing edge of Ia decays more rapidly at slow scan rate than predicted by theory, the film is apparently passivating in nature; this is supported by the depressed a.c. capacitive current at potentials positive of Ia when R^- is present. At fast scan rate, the amount of deposited film is insufficient to cause passivation, e.g., Ia in curve 2 of Fig. 3B, which has the theoretical shape for film formation, corresponds to a deposition equivalent of ca. 50 μC cm^{-2} (from foot of peak to E_λ).

CPK molecular models [25] were used to estimate the molecular dimensions of uracil. Assuming a flat orientation of R^- on the electrode surface, the area of a circle with a diameter equal to the O(2) to H(5) distance of 7.4 Å is 43.0 Å^2; for this as the molecular swept area, the maximum monolayer coverage is 3.9×10^{-10} mol cm^{-2} or 37 μC cm^{-2} for R^-. For the perpendicular orientation, the molecular thickness perpendicular to the ring, 3.1 Å, was multiplied by the molecular diameter parallel to the electrode surface, 7.0 Å (if the N(1) or either O sits on the surface); the product, 21.7 Å, assumes a rigid, unswept area for close packing and gives a maximum monolayer coverage of 7.7×10^{-10} mol cm^{-2} or 74 μC cm^{-2} for R^-. Since Q/A reaches a limiting value of 70 to 80 μC cm^{-2}, the charge passed in peak Ia corresponds to two layers of R^- deposited in a flat orientation or a monolayer in a perpendicular orientation.

Figure 7 indicates that the amount of mercury-uracil salt reduced in peak IIc, Q_c, is less than that deposited in peaks Ia and IIa, Q_a; however, the fraction of deposited salt which is reduced in IIc approaches unity at low surface coverages. Since Fig. 1 indicates that, in the region from 0.6 to 1 mM uracil, the effect of the chemical reaction is only slightly concentration-dependent, the relation between Q_a and added TEAH is that which would be theoretically expected, i.e., at 0.40 mM TEAH, Q_a should equal 0.40/0.94 times Q_a at 0.94 mM TEAH plus 0.6 times Q_a at 0.0 mM TEAH; the observed deposited charge densities at 0.40 mM, 199 and 140 μC cm^{-2} at 0.11 and 0.28 V s^{-1}, respectively, are in good agreement with the expected values of 198 and 131 μC cm^{-2}, respectively.

It is unlikely that the Q_c/Q_a ratios less than unity are due to oxidative formation of a soluble species, since the E_p for Ia and IIa predict K_{sp} of 10^{-29} M^3 and 10^{-19} M^3, respectively, for Hg(I) salts; at 0.94 mM TEAH, the difference between Q_a and Q_c for a 0.11 V s^{-1} scan rate would represent a concentration of Hg(I) which was eighteen orders-of-magnitude larger than that allowed by the larger K_{sp}, if the soluble Hg(I) were contained within an 0.1-cm region of the electrode surface. The probable reason for Q_c/Q_a less than one is the number of layers of salt deposited by Ia and IIa (Table 3). Regardless of which orientation is assumed

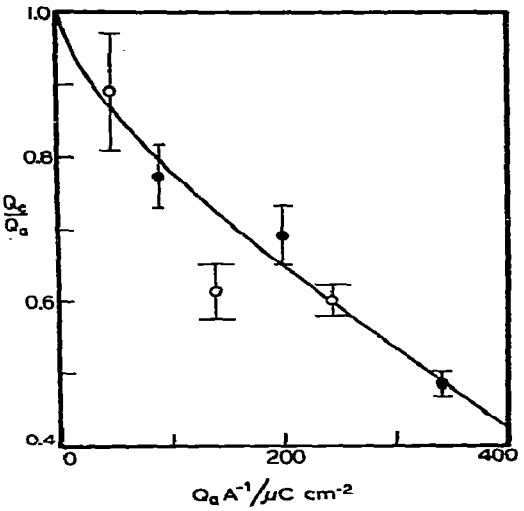

Fig. 7. Relation between amount of mercury-uracil salt reduced in cyclic peak IIc (Q_c) and amount deposited in cyclic peaks Ia and IIa (Q_a). Conditions: 1.00 m*M* uracil; 0.0153 cm^2 electrode area; solid circles, 0.11 V s^{-1} scan rate; open circles, 0.28 V s^{-1} scan rate. The three points at each scan rate represent, with increasing Q_a, 0.0, 0.40 and 0.94 m*M* TEAH added, respectively.

for the uracil ring relative to the electrode at 0.94 m*M* TEAH, four or more layers of uracil anion are deposited by Ia and IIa. Two possible explanations can be advanced for the cause of small Q_c/Q_a. Firstly, the deposition of more than a monolayer of salt may result in loss of portions of subsequent layers

TABLE 3

Number of layers of uracil anion deposited by cyclic peaks Ia and IIa (m_a) and stripped from the electrode surface by peak IIc (m_c) as a function of scan rate, amount of added base and assumed orientation [a]

[TEAH]/m*M*	Parallel [b]		Perpendicular [b]	
	m_a	m_c	m_a	m_c
0.0 [c]	2.4	1.8	1.2	0.9
0.40 [c]	5.8	3.7	2.7	1.9
0.94 [c]	9.2	4.4	4.6	2.2
0.0 [d]	1.3	1.1	0.6	0.6
0.40 [d]	3.9	2.3	1.9	1.2
0.94 [d]	6.6	3.9	3.3	2.0

[a] Data are based on integrated area of cyclic voltammetric peaks for 1.00 m*M* uracil (cf. Experimental for method of peak area evaluation); assumed molecular dimensions for conversion from total charge under peaks to m_a or m_c are given in Mechanism discussion of mercury-uracil salt nature; electrode area was 0.0153 cm^2.
[b] Assumed orientation of the plane of the uracil ring relative to the electrode surface.
[c] Scan rate was 0.11 V s^{-1}.
[d] Scan rate was 0.28 V s^{-1}.

through non-adherence to the electrode surface, i.e., the binding force between two layers of mercury-uracil salt may be weak. Alternatively, because of the passivating nature of a monolayer (cf. previous discussion), it is very possible that only the first one to two layers of salt are reduced, while the remaining layers are dislodged and fall into solution when the first layers are reduced.

Because it is more reasonable to assume that peak IIc represents reduction of up to two layers rather than four layers, particularly since, at 0.94 m*M* TEAH, IIc is actually two slightly resolved peaks, the uracil is likely deposited in a perpendicular orientation; hence, the monolayer thickness is ca. 7.5 Å with the uracil anions closely packed, which likely yields considerable resistance to diffusion of the requisite mercury ions for subsequent layers. The passivating nature of a monolayer is likely due to the necessity for mercury ions to diffuse through the closely packed monolayer to form subsequent layers.

Assuming a 2.5 Å diameter for the mercurous ion, two layers represent a film thickness of ca. 17—18 Å. The four to five layers deposited at 0.94 m*M* TEAH would represent a film thickness of 38 to 48 Å. Since the principal cohesive force between layers is probably a weak interaction between the mercury ion and oxygen on the uracil in an adjacent layer, a film thickness of 40 to 50 Å is unlikely; hence, much of the film is probably lost by detachment.

The disappearance of IIa at fast scan can be explained in two manners. (a) Both Ia and IIa are due to deposition of the same mercury salt. At slow scan, the electrode is passivated by Ia before the R^- surface concentration reaches zero. At sufficiently positive potential, the passivation is overcome and further deposition occurs, e.g., IIa. At fast scan, the surface concentration of R^- is driven to zero by Ia without passivation; hence, no additional deposition peak is observed. (b) The deposition due to Ia and IIa represent different mercury salts. As previously mentioned, the uracil anion exists as a mixture of the forms deprotonated at N(1) and N(3); since the mercury salts of these two R^- forms probably have different solubilities, two deposition peaks would be expected. The absence of two film stripping peaks means that a rearrangement occurs to produce one stable mercury salt. The absence of IIa at fast scan must be due to kinetic control of the IIa process, which shifts positive of the positive background discharge at fast scan.

The behavior at low concentrations of R^- is not consistent with Ia and IIa being due to the same process. IIa appears at concentrations of R^- for which Ia is considerably below its limiting value; however, this behavior is consistent with salt formation involving different anionic uracil tautomers.

Digital simulation

Digital simulation [27] permits comparison between the experimentally observed faradaic behavior and that predicted for the mechanism in Fig. 6. Simulations of the reaction of eqn. (2) at an expanding plane (DME), which assume that dimerization of $\dot{R}H_2$ is sufficiently rapid to consume all $\dot{R}H_2$ by non-faradaic means, thus making the protonation of $\dot{R}H^-$ irreversible, indicate good agreement between experimental and theoretical behavior for $k_1 = 10^4\ M^{-1}\ s^{-1}$ (Fig. 1). However, as expected, simulated cyclic voltammograms predict that $i_{pc}/Acv^{1/2}$ increases with increasing v (Table 4) and that the chemical step is outrun by

TABLE 4

Comparison of experimental and simulated current behavior on cyclic voltammetry of uracil

Reaction	v/V s^{-1}	$i_{pc}/Acv^{1/2}$ [b]		i_{pa}/i_{pc} [c]
		Experimental	Simulated	
2 [a]	0.10		387	0.0
	0.13	226		
	1.0		509	0.73
	1.3	220		
	10.0		562	0.96
	13.0	210		
3 [d]	1.0		315 [e]	
			350 [f]	
	1.3	220		
	10.0		389 [e]	
			433 [f]	
	13.0	210		

[a] Simulation is for reaction (2) with $k_1 = 10^4\ M^{-1}\ s^{-1}$ and 1 mM uracil.
[b] Units are $\mu A\ s^{1/2}\ mM^{-1}\ V^{-1/2}\ cm^{-2}$; i_{pc} is the peak current for peak Ic.
[c] Ratio of the simulated peak current for oxidation of RH^- to that for reduction of RH. Experimental ratio is zero in all cases.
[d] Simulation is for reaction (3) with $k_1 = 10^6\ M^{-1}\ s^{-1}$ and 1 mM uracil.
[e] Assumed that $k_2 = 10^4\ M^{-1}\ s^{-1}$.
[f] Assumed that $k_2 = 10^6\ M^{-1}\ s^{-1}$.

$v = 10$ V s^{-1}, i.e., as v increases from 0.1 to 10 V s^{-1}, the i_{pa}/i_{pc} ratio increases from 0.0 to 1.0.

$$RH \underset{-e}{\overset{+e}{\rightleftharpoons}} \dot{R}H^- \xrightarrow[k_1]{+RH} \dot{R}H_2 + R^- \qquad (2)$$

The predicted ability to outrun the protonation totally at such scan rates for $k_1 = 10^4\ M^{-1}\ s^{-1}$ is due to faradaic consumption of the protonating agent, RH. As v is increased, the surface concentration of RH is driven to zero far more rapidly than diffusion can supply RH, so that not only is the time for protonation decreased, i.e., time to scan through the peak, but the protonation rate is slowed by the decreased RH supply.

Addition of the dimerization of $\dot{R}H^-$ to the simulation mechanism, i.e., reaction of eqn. (3), increases the rate of $\dot{R}H^-$ disappearance and requires a larger value of k_1 to predict the observed I_d—c behavior, i.e., the amount of RH consumed by a non-faradaic process.

$$RH \underset{-e}{\overset{+e}{\rightleftharpoons}} \dot{R}H^- \xrightarrow[k_1]{RH} \dot{R}H_2 + R^- \qquad (3)$$
$$\downarrow k_2$$
$$0.5\ (RH)_2^{2-}$$

Although the predicted cyclic voltammetric behavior (Table 4) for reaction scheme (3) deviates less from experimental results than does reaction scheme (2), $i_{pc}/Acv^{1/2}$ still increases with v. Simulation of d.c. polarography for reaction

(3) using $k_1 = 10^6\ M^{-1}\ s^{-1}$ and $k_2 = 10^4\ M^{-1}\ s^{-1}$ predicts an I_d of 0.85 for a 0.08 mM solution; 1.42 is observed. Decreasing k_1 to $10^5\ M^{-1}\ s^{-1}$ increases I_d to 0.99. Thus, to obtain agreement between the observed DME behavior at low uracil concentration and the cyclic results at high uracil concentration, it is necessary to assume that $\dot{R}H_2$ is electroactive at the uracil reduction potential. At low uracil concentration, the rate of protonation will be slow, so that most RH is available for reduction; the dimerization of $\dot{R}H_2$ will also be slow, permitting a significant fraction of the $\dot{R}H_2$ formed to be further reduced to RH_2^-; i_l will then approach the magnitude for a net transfer of one electron per uracil molecule. At high uracil concentration, dimerization of $\dot{R}H_2$ will be fast and reduction of $\dot{R}H_2$ will not contribute significantly to the observed faradaic current.

The electroactivity of $\dot{R}H_2$ at the potential required for the initial 1e reduction of RH would be in conformity with such e.c.e. reactions, e.g., reduction of pyrimidine itself in non-aqueous media on proton donor addition [14].

The decrease in experimental $i_{pc}/Acv^{1/2}$ with increasing v may be due to a finite electron-transfer rate. The trend of E_{pc} with v is indicative of a non-reversible electron-transfer. For 1.25 mM uracil, dE_p/d (log v) is −58 mV, compared to −20 mV expected for a reversible electron-transfer process [28] (at v = 10 V s^{-1}, the expected slope of $-E_p$ vs. log v for $k_2 < 10^5\ M^{-1}\ s^{-1}$ will be less than 20 mV $decade^{-1}$). For a charge-transfer with a small standard heterogeneous rate constant ($k_{s,h}$) and a following dimerization, the predicted E_p—log v slope is −59 mV $decade^{-1}$ [28], e.g., for $k_2 = 10^6\ M^{-1}\ s^{-1}$, a $k_{s,h} \leqslant$ ca. 0.005 cm s^{-1} is necessary to achieve a slope of −59 mV $decade^{-1}$, which is essentially identical to the observed −58 mV $decade^{-1}$.

The protonation step in reaction (2) is observed in the simulations to have some effect on E_p. The difference of $\Delta E = E_p - E_c^\circ$ changes from −1 mV at v = 0.1 V s^{-1} to −21 mV at 1 V s^{-1} and −27 mV at 10 V s^{-1}. For reaction (3) with $k_1 = 10^4\ M^{-1}\ s^{-1}$, ΔE changes from 27 mV at 1 V s^{-1} to −1 mV at 10 V s^{-1} for $k_2 = 10^4\ M^{-1}\ s^{-1}$, and from 19 mV at 1 V s^{-1} to −3 mV at 10 V s^{-1} for $k_2 = 10^6\ M^{-1}\ s^{-1}$. These shifts of E_p for the simulated data do not agree with the experimentally observed dE_p/d (log v) values, possibly because the simulations assume a reversible electron-transfer.

Although the reduction of uracil may occur at a finite rate, the large number of parameters available for variation ($k_{s,h}$, α, k_1, k_2, k_3) precludes elucidation of a unique kinetic mechanism by digital simulation; however, simulations do verify the ability of a reaction scheme involving protonation of $\dot{R}H^-$ by RH to describe the observed I_d—c behavior.

Calculated and experimental ease of reduction

Molecular orbital calculations using the CNDO/2 technique [29] yield energy levels for the lowest empty molecular orbital (LEMO) of 2.78 eV for pyrimidine [30], 2.85 eV for cytosine [31], and 2.25 eV for the lactam form of uracil [31]. These calculations, which predict that cytosine should be reduced 0.07 V more negative than pyrimidine and uracil ca. 0.5 V more positive than either pyrimidine or cytosine, do not account for differences in solvation state or effects of coupled reactions.

In both acetonitrile (AN) and dimethylformamide (DMF), $E_{1/2}$ for pyrimidine is —2.34 V [15]. (All potentials cited are vs. aqueous SCE and generally refer to the initial 1*e* reduction.) In DMSO, $E_{1/2}$ is —2.37 V for cytosine [17] and —2.3 V for uracil. The observed 0.03-V difference in ease of reduction of cytosine and pyrimidine is in good agreement with the calculated LEMO energy difference. However, there is a 0.5-V discrepancy between the predicted and observed differences between uracil and either pyrimidine or cytosine. Two possibilities are apparent: (a) Differences in coupled chemical reactions or solvation effects make pyrimidine and cytosine more easily reducible by ca. 0.5 V compared to uracil than the LEMO energy predicts. (b) Differences in coupled chemical reactions, a non-reversible electron-transfer, or solvation effects make uracil more difficult to reduce by about 0.5 V compared to pyrimidine and cytosine than predicted by the LEMO calculations.

Solvation effects do not seem a probable cause because of the relative independence of $E_{1/2}$, e.g., for pyrimidine, of solvent nature and because solvation effects on the ease of reducibility are generally significant only if the oxidized and reduced forms are differently solvated [32], which is unlikely for the pyrimidines.

Preceding chemical reactions can be eliminated as the cause of a more difficultly reducible uracil species because of evidence against the likely reaction types: protonation, self-association, and tautomerism. The ineffectiveness of added proton donor on the ease of uracil reduction indicates the absence of a necessary prior protonation. A preceding association reaction is unlikely because (a) self-association would result in a concentration-dependent diffusion coefficient but D is concentration-independent as indicated by the agreement between coulometric n and polarographic I_d values at high and low concentrations, and (b) studies of the concentration and solvent dependence of n.m.r. chemical shifts for substituted uracil [23] indicate uracil to be strongly hydrogen bonded to DMSO and not to self-associate to any significant extent. Since the lactam tautomer predominates in solution, a preceding tautomeric reaction, i.e., reduction occurring only via a minor tautomer, would not cause a 0.5-V overpotential unless some other factor hindered reduction of the lactam form, i.e., calculated LEMO energies [31] are 2.42 and 2.12 eV for the 2-hydroxy lactims protonated at N(1) and N(3), respectively, 1.94 eV for the 4-hydroxy lactim protonated at N(1), and 3.22 eV for the dilactim. Additionally, if reduction occurred via one of the minor tautomers, all of which have at least one ring nitrogen site available for protonation, proton donor addition should facilitate reduction, which is not experimentally observed.

The remaining possibility is a non-reversible uracil reduction, with some difference in the rates of following chemical reactions from those for pyrimidine and cytosine. If the 0.5-V overpotential were solely due to a totally irreversible electron-transfer with a transfer coefficient (α) of 0.5, $k_{s,h}$ would be 1×10^{-7} cm s^{-1} [33]. Such a small value for $k_{s,h}$ seems unlikely, particularly in light of the fact that pyrimidine reduction appears to involve a reversible — or, at least, very rapid — electron transfer [15].

The results in Fig. 4 for high concentration and rapid scan rate are considerably below the 268 μA $s^{1/2}$ mM^{-1} $v^{-1/2}$ cm^{-2} expected for $i_p/Acv^{1/2}$, assuming a reversible, 1*e* reduction of half of the uracil. To correct the data in Fig. 4 for the

effects of electrode sphericity, the spherical contribution to $i_p/Acv^{1/2}$ was calculated and subtracted from the observed $i_p/Acv^{1/2}$ to yield the planar term of $i_p/Acv^{1/2}$ [11]. The spherical correction is significant at slow scan, i.e., less than 1 V s^{-1}, so that, for example, the planar $i_p/Acv^{1/2}$ values corresponding to 0.2 m*M* at a v of 0.1 V s^{-1} are 380 and 399 (cf. Fig. 4); a plot of the planar $i_p/Acv^{1/2}$ for 0.2 m*M* yields an intercept of 406 at $v = 0$. The decrease in planar $i_p/Acv^{1/2}$ at 0.2 m*M* from 406 at $v = 0$ to 278 at 32 V s^{-1} is that expected by assuming a reversible electron-transfer at infinitely slow scan rate and an irreversible electron-transfer with an α of 0.39 at rapid scan rate for reduction of 75% of the uracil in both cases. The fast scan rate limit at 1.25 m*M*, 187, also corresponds to an irreversible electron-transfer with an α of 0.39, assuming 50% of the uracil to be reduced. Although the complex nature of the apparent mechanism precludes quantitative evaluation of the heterogeneous kinetic parameters, the foregoing facts indicate that the experimental results are not at variance with a finite electron-transfer rate.

Sites of electron entrance and residence

Reduction of pyrimidine, 2-HP and cytosine in aqueous and non-aqueous media indicates that the electron initially enters at C(4) when the 3,4 N=C is present [3]. In aqueous media, the second most likely reduction site is the 1,2 N=C when present [3]; however, the possibility has been noted [14] of rapid electron rearrangement after initial electron addition to pyrimidine in AN. Thus, the structure of detectable intermediates and final products is not conclusive regarding the site of electron injection.

Hayon [34] concluded, on the basis of spectral data for the protonated radicals formed in reduction of uracil by pulse radiolysis in aqueous media, that the solvated electron, e_{sol}, entered uracil at C(2) and C(4); he postulated that in pH 5 solutions species (III) and (IV) are formed (after protonation) and that in alkaline solution (up to 0.3 *M* NaOH), species (V) is formed.

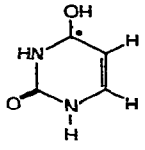
(III)

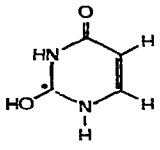
(IV)

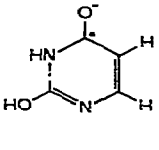
(V)

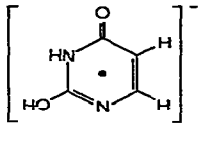
(VI)

Grimison and Eberhardt [35] noted that the LEMO is delocalized over the entire uracil molecule and that, since e_{sol} is a special type of radical, one can only say that e_{sol} enters the LEMO, i.e., the atomic site of charge injection cannot be deduced from the resident site of the unpaired electron on the radical; however, based on theoretical calculations, they predicted that species (III) would be formed on pulse radiolysis in neutral solution and species (VI) in alkaline solution. Although Hayon postulated species (III) and (IV) in neutral media to explain both his near- and far-ultraviolet spectra of pulse radiolysis intermediates, Grimison and Eberhardt calculated that the species (III) spectrum is consistent with both the near- and far-ultraviolet observed behavior; thus, the pulse radiolysis data indicate that injected electron residence is at C(4) and that protonation in aqueous medium is at O(4).

Photochemical reactions have been either postulated or proven to involve attack at 5,6 C=C [36—38]. Irradiation of uracil solutions has been reported to yield 5,6-dihydrouracil [37]. E.p.r. studies of ultraviolet-irradiated aqueous uracil solutions indicate that (VII) is formed; when H_2O_2 is present, (VIII) is formed at pH 1 to 7 and (IX) at pH 8 to 10 [38].

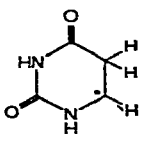

(VII)

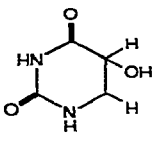

(VIII)

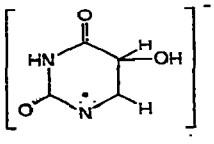

(IX)

Theoretical electron densities for the lactam form of uracil indicate that of the four carbons, C(2) is most electron deficient with a net charge of +0.45 (average of values on p. 276 of ref. 7, excluding values from EHT and IEHT methods) while C(4) is second most deficient (net charge = +0.34). The net charges on C(5) and C(6) are —0.15 and +0.13, respectively; hence, C(2) or C(4) appears to be the logical reduction site.

The observed catalytic hydrogen discharge induced by uracil on acid addition to DMSO solutions suggests that electrochemical reduction proceeds via the predicted path for pulse radiolysis reduction, i.e., electron injection at C(4), rather than by the photochemical path involving 5,6 C=C reduction. Catalytic hydrogen discharge generally involves a nitrogen or oxygen site to which an acid can hydrogen bond; this involves either a basic nitrogen or, more likely, C=O. If electrochemical reduction occurred at 5,6 C=C, proton addition or hydrogen bonding to the reduced site would not produce a likely configuration for catalytic hydrogen discharge; however, reduction at C(4) followed by proton addition or hydrogen bonding to O(4) would yield structure (III), which has been postulated as the pulse radiolysis intermediate and which is ideal for catalytic hydrogen discharge. Reduction of the proton at O(4) might yield structure (VI), which is the postulated pulse radiolysis product in basic medium. If structure (VI) is formed on reduction, then hydrogen bonding and catalytic discharge can occur at N(1).

Since calculations indicate the LEMO to be a π-orbital and since uracil is virtually a planar molecule, reduction would probably occur with the plane of the ring parallel to the electrode surface; however, because of the high electron densities on the two oxygens (a net charge of ca. —0.4 on each (p. 276 of ref. 7)), there may be considerable electrostatic repulsion between the oxygens and the very negatively charged electrode surface. This repulsion may result in (a) a required stereochemical structure for the unreduced state which significantly raises the LEMO energy and, thereby, hinders reduction, and (b) a molecular structure for the activated state which raises the energies of the occupied orbitals and, therefore, produces a large energy barrier to reduction. If electron injection occurs at either C(2) or C(4), then an additional possible source of energetic hindrance is the magnitude and orientation of uracil's permanent dipole moment, which is 4.0 ± 1.3 *D* with an angle of 71° relative to the N(1)—C(4) axis and toward N(3) [39]. In the presence of a large electric field gradient such as that at a solution/electrode interface, the most stable orientation for the uracil molecule will be with C(2) and C(4) away from the electrode and with the ring's plane aligned to the electric field; thus, considerable activation energy may

be necessary to orient C(2) or C(4) near the electrode, if one of these is the site of electron entrance. Additionally, if reduction occurs with the ring plane parallel to the surface, then the molecule's permanent dipole must be oriented perpendicular to the electric field, which requires considerable energy.

The foregoing information indicates that the most probable site for reduction is either C(2) or C(4); based on initial studies of thymine (5-methyluracil) in DMSO [40], C(4) appears to be the site of electron residence. Although the postulated reduction site and orientation permit energetic arguments which could explain a slow electron-transfer, there is no conclusive experimental evidence for a slow electron-transfer step; such a slow step would be at variance with data for other pyrimidines, for which the initial electron-transfer appears to be reversible. Because of the complexity of the uracil reduction mechanism and the absence of available theories for data evaluation, the electron-transfer rate cannot be measured at present.

CONCLUSIONS

Uracil reduction is analogous to the 2-HP reduction mechanism, in that the radical anion abstracts a proton from the parent compound to form the parent compounds's conjugate base and the free radical, which rapidly dimerizes (Fig. 6). The protonation reaction is considerably more rapid than the radical anion dimerization; the high-concentration polarographic I_d indicates that not more than 8% of the radical anion is removed by dimerization, whereas at least 92% is removed by protonation. The rapid free radical dimerization makes the protonation step effectively irreversible. A rapid protonation rate is consistent with the strong proton affinity of radical anions and the lack of charge repulsion between reacting molecules. The strong basicity of the radical anion is also evident from the fact that a very weak acid, uracil, is the protonating agent in such a rapid reaction.

Digital simulations indicate that the protonation rate constant is at least 10^5 M^{-1} s^{-1}, assuming the rate of radical anion dimerization to exceed 10^4 M^{-1} s^{-1}. The simulations also indicate that consistency between cyclic voltammetric and d.c. polarographic results requires that, at low concentration, some free radical be further reduced, rather than dimerizes.

Although the experimental results are consistent with a quasi-reversible electron-transfer and a transfer coefficient of 0.4, which would partially explain the observed trend in ease of reduction of various pyrimidines compared to the theoretically predicted ease of reduction, the uracil reduction mechanism is too complex to permit quantitative electron-transfer evaluation from presently available theory.

The uracil anion, as expected, is much more difficultly reducible than uracil itself and its reduction is not observed within the available potential range.

The interaction of uracil anion with mercury is consistent with previous reports and with electrochemical results for the similar compound, 2-hydroxypyrimidine. Experimental results indicate formation of a Hg(I)-uracil salt with the plane of the uracil ring perpendicular to the electrode surface. A maximum of two layers is stripped electrochemically; the fraction of salt lost by mechanical detachment increases with increasing salt deposit. The presence of two anodi

peaks for film deposition, but only one peak for film stripping, indicates that two mercury-uracil salts are involved, differing in the site of deprotonation, i.e., N(1) or N(3), and that one of the salts is not stable; hence, proton rearrangement within the crystal structure to form the other, stable mercury salt probably occurs.

Although results with added acids do not permit verification of the added proton donor's substitution for uracil as a protonating agent, the results do preclude, as expected from predominance of uracil in the lactam tautomeric form, any protonation step preceding reduction. Additionally, the occurrence of catalytic hydrogen reduction on acid addition, which generally is due to protonation or hydrogen-bonding to a basic nitrogen or, preferably, to a carbonyl group, indicates that reduction occurs at C(4), as has been observed on pulse radiolysis of uracil; reduction of the 5,6 C=C bond, observed in photochemical experiments, would not be expected to result in a species which catalyzed hydrogen reduction. Reduction at C(4) would be consistent with observed electrochemical behavior for other pyrimidines.

ACKNOWLEDGMENTS

The authors thank the National Science Foundation and the Horace H. Rackham School of Graduate Studies of The University of Michigan, which helped support the work described.

REFERENCES

1 A.L. Underwood and J.N. Burnett in A.J. Bard (Ed.), Electroanalytical Chemistry, Vol. 6, Marcel Dekker, New York, 1972, pp. 1—85.
2 P.J. Elving, J.E. O'Reilly and C.O. Schmakel in D. Glick (Ed.), Methods of Biochemical Analysis, Vol. 21, Interscience, New York, 1973, pp. 287—465.
3 P.J. Elving in G. Milazzo (Ed.), Topics in Bioelectrochemistry and Bioenergetics, Vol. I, John Wiley, London, 1976, pp. 179—286.
4 J. Komenda, Symposium on Electrochemical Analysis of Nucleic Acids, Lisensky Dvur, Czechoslovakia, May 14—17, 1975, Abstracts, p. 9.
5 A.L. Lehninger, Biochemistry, Worth, New York, 2nd edn., 1975, p. 316.
6 T. Wasa and P.J. Elving, J. Electroanal. Chem., 91 (1978) 249.
7 J.S. Kwiatkowski and B. Pullman in A.R. Katritzky and A.J. Boulton (Eds.), Advances in Heterocyclic Chemistry, Vol. 18, Academic Press, New York, 1975, pp. 199—335.
8 J.P. Kokko, J.H. Goldstein and L. Mandell, J. Amer. Chem. Soc., 83 (1961) 2909.
9 D.A. Hall and P.J. Elving, Anal. Chim. Acta, 39 (1967) 141.
10 H. Matsuda, Bull. Chem. Soc. Jap., 26 (1953) 342.
11 T.E. Cummings and P.J. Elving, Anal. Chem., 50 (1978) 480.
12 N. Yao and D.N. Bennion, J. Electrochem. Soc., 118 (1971) 1097.
13 D.L. Smith and P.J. Elving, J. Amer. Chem. Soc., 84 (1962) 2741.
14 J.E. O'Reilly and P.J. Elving, J. Amer. Chem. Soc., 93 (1971) 1871.
15 J.E. O'Reilly and P.J. Elving, J. Amer. Chem. Soc., 94 (1972) 7941.
16 J.W. Webb, B. Janik and P.J. Elving, J. Amer. Chem. Soc., 95 (1973) 991.
17 T. Wasa and P.J. Elving, unpublished results.
18 A.R. Katritzky and A.J. Waring, J. Chem. Soc., (1962) 1540.
19 B. Janik and P.J. Elving, Chem. Rev., 68 (1968) 295.
20 O. Manousek and P. Zuman, Collect. Czech. Chem. Commun., 20 (1955) 1340.
21 N. Nakanishi, N. Suzuki and P. Yamazaki, Bull. Chem. Soc. Jap. 34 (1961) 53.
22 R. Shapiro and S. Kang, Biochim. Biophys. Acta, 232 (1971) 1.
23 L. Katz and S. Penman, J. Mol. Biol., 15 (1966) 220.

24 J.A. Carrabine and M. Sundaralingana, Biochemistry, 10 (1971) 292.
25 CPK Precision Molecular Models, The Ealing Corporation, 2225 Massachusetts Ave., Cambridge, Mass. 02140, U.S.A.
26 P. Delahay, New Instrumental Methods of Analysis, Interscience, New York, 1954, pp. 123—125.
27 S. Feldberg in A.J. Bard (Ed.), Electroanalytical Chemistry, Vol. 3, Marcel Dekker, New York, 1966, pp. 199—296.
28 L. Nadjo and J.M. Saveant, J. Electroanal. Chem., 48 (1973) 113.
29 J.A. Pople and G.A. Segal, J. Chem. Phys., 44 (1966) 3289.
30 D.M.W. van der Ham, G.F.S. Harrison, A. Spaans and D. van der Meer, Rec. Trav. Chim., 94 (1975) 168.
31 B.L. Lesyng, M. Sci. Thesis, Univ. of Warsaw, 1972, and unpublished results (cited in ref. 7).
32 M.E. Peover in A.J. Bard (Ed.), Electroanalytical Chemistry, Vol. 2, Marcel Dekker, New York, 1967, pp. 1—51.
33 J. Heyrovsky and J. Kuta, Principles of Polarography, Academic Press, New York, 1966, p. 213.
34 E. Hayon, J. Chem. Phys., 51 (1969) 4881.
35 A. Grimison and M.K. Eberhardt, J. Phys. Chem., 77 (1973) 1673.
36 C. Nofra and A. Cier in B. Pullman (Ed.), Electronic Aspects of Biochemistry, Academic Press, New York, 1964, pp. 405—7.
37 D. Elad and I. Rosenthal, Chem. Commun., (1968) 879.
38 J.K. Dohrmann and R. Livingston, J. Amer. Chem. Soc., 93 (1971) 5363.
39 R.F. Stewart, J. Chem. Phys., 53 (1970) 205.
40 T.E. Cummings, M.H. Hyman and P.J. Elving, unpublished results.